INTERNATIONAL ATOMIC ENERGY AGENCY
UNITED NATIONS EDUCATIONAL, SCIENTIFIC AND CULTURAL ORGANIZATION

INTERNATIONAL CENTRE FOR THEORETICAL PHYSICS
34100 TRIESTE (ITALY) - P.O.B. 586 - MIRAMARE - STRADA COSTIERA 11 - TELEPHONES: 224281/2/3/4/5/6
CABLE: CENTRATOM - TELEX 460392-1

SMR/100 - 25

WINTER COLLEGE ON LASERS, ATOMIC AND MOLECULAR PHYSICS

(24 January - 25 March 1983)

Vibration-Rotation Spectroscopy of the HD^+ Ion near the Dissociation Limit

A. CARRINGTON

Department of Chemistry
University of Southampton
Southampton SO9 5NH
U.K.

MOLECULAR PHYSICS, 1981, VOL. 44, NO. 2, 267–285

Vibration–rotation spectroscopy of the HD^+ ion near the dissociation limit

I. Experimental methods and measurements of the $v = 18$–16 band

by ALAN CARRINGTON and JULIET BUTTENSHAW
Department of Chemistry, University of Southampton, Hampshire SO9 5NH, England

(*Received* 13 *May* 1981 ; *accepted* 2 *June* 1981)

A new method of detecting vibration–rotation transitions in the HD^+ ion is described. The technique uses an ion beam and relies upon the detection of infrared photodissociation of levels close to the dissociation limit of HD^+. These levels are populated by the electron impact ionization process and measurements of nine rotational components of the $v = 18$–16 band are described. The results reveal small but systematic discrepancies in the best available theoretical values of the relative energies of these vibration–rotation levels. The resolution of structure arising from proton hyperfine interaction is also described.

1. INTRODUCTION

The HD^+ ion is the simplest molecule which can have an electric dipole allowed vibration–rotation absorption spectrum. The hydrogen molecular ion has been the subject of many theoretical studies and since the difficulties arising from interactions between electrons are absent, the electronic and nuclear wavefunctions and energies can be calculated very accurately. The hydrogen molecular ion is much more elusive in the laboratory, however, and very few experimental measurements can match the theory in accuracy. Apart from the work described in this paper we are aware of only two types of spectroscopic study which meet this criterion. In 1962 Dehmelt and Jefferts [1] described an ingenious method of producing spatial alignment of the hydrogen ion by selective photodissociation, and Richardson *et al.* [2] showed that radiofrequency transitions could be detected through their effects on the spatial alignment. In subsequent papers Jefferts [3] measured nuclear hyperfine transitions for the lower rotational levels of the vibrational levels $v = 4$ to 8, achieving linewidths of a few kHz with corresponding precision in the determination of the hyperfine constants. These experiments used quadrupole radiofrequency traps to hold the ions for periods up to 1 s, and relied on spatial alignment arising from photodissociation produced by polarized white light.

The first detection of vibration–rotation transitions in the HD^+ ion was described in 1976 by Wing *et al.* [4]. They used a carbon monoxide infrared laser as the radiation source, employed Doppler tuning of an HD^+ ion beam to scan the spectrum, and charge–exchange reactions to provide a detection mechanism. In this method the HD^+ ion beam intensity is monitored continuously

0026–8976/81/4402 0267 $02·00

and the beam attenuated by introduction of a suitable neutral gas (for example, hydrogen) which undergoes charge–exchange with the ions. Vibrational excitation of the ion beam resulting from infrared absorption produces a change in the cross-section for charge–exchange, and consequently is detected as a change in the HD^+ ion beam intensity. Wing *et al.* detected vibration–rotation transitions involving $v=0$ to 3 and $N=0$ to 2, determining the transition frequencies to an accuracy of 0·001 cm^{-1}.

Our method which has been reported briefly elsewhere [5] but which is described in detail in this paper, involves the infrared photodissociation of an HD^+ beam, and the detection of changes in the photofragment ion yield (H^+ or D^+) arising from excitation of vibration–rotation transitions. The technique is very sensitive and makes possible the study of vibrational levels which are close to the dissociation limit, even though the populations of these levels in the HD^+ beam are very low. It is for just these levels that even the most comprehensive theoretical calculations might become inaccurate because of the difficulties associated with the separation of electronic and nuclear motions. As our work has progressed we have become increasingly aware of certain fundamental aspects of molecular physics which are not well understood but which are amenable to experimental investigation in this, the simplest of all molecules. We return to some of these aspects in the final section of this paper.

2. Principles

Our experiments make use of ion beams and employ many of the established techniques of mass spectrometry. From the viewpoint of molecular spectroscopy an ion beam is a novel medium with a number of unusual features, some of which are advantageous. These features have been discussed elsewhere by Carrington [6] and will be reviewed only briefly here. The ions are created by electron impact on an appropriate target gas and are extracted from the source by acceleration to potentials of several kilovolts to form a well collimated beam. In our experiments on HD^+ the ion velocities range from $2{\cdot}5\times10^5$ m s^{-1} to 8×10^5 m s^{-1} and since the distance from the source to the final detector is close to 3 m, the ion transit times range from 4 to 12 μs. During this time the ions enjoy a collision-free environment so that there is little opportunity for relaxation effects to occur. Consequently provided the ion source pressure is low enough to preclude collisions before acceleration, the internal energy distribution of the ions in the beam is that produced by the electron impact ionization process itself. This is an important aspect which is generally advantageous, and on which the success of our technique depends.

In our apparatus the most intense HD^+ ion beams obtainable are about 10^{-7} A, corresponding to a beam flux of 6×10^{11} ions s^{-1}. Bearing in mind the rapid transit of the ions through an electromagnetic radiation field, the instantaneous ion density is so low that attempts to perform absorption spectroscopy by the traditional methods have little chance of success. Consequently most approaches to the spectroscopy of molecular ion beams are based upon the principle that one monitors the intensity of either the parent ion beam or a secondary fragment ion beam, and looks for changes produced as a result of the absorption of radiation. As we outlined in the introduction, the successful detection of an infrared

absorption spectrum of HD^+ by Wing *et al.* [4] made use of the dependence of the cross-section for charge–exchange on the vibrational state of the ion. Our technique relies upon corresponding changes in the cross-section for infrared photodissociation. In the change–exchange method changes in the parent ion intensity are measured; the method is therefore analogous to a spectroscopic absorption experiment. In our experiments photofragment ions arising from prior vibrational excitation of the ions are detected; the method is closer, therefore, to a spectroscopic emission experiment and is consequently more sensitive. It necessarily probes the higher vibrational levels of the ion, however, so that the charge–exchange and photodissociation methods are entirely complementary.

The ion source in our apparatus is maintained at a temperature between 200 and 350°C so that the inlet gas, neutral HD, is essentially in its vibrational ground state and with a rotational level population determined by the Boltzmann distribution law. The electron impact ionization process, however, creates HD^+ ions in which all the vibrational levels of the ground electronic state are populated. This is because the potential energy curve for the ion is displaced to longer internuclear distances relative to that of the neutral molecule. Several authors have described calculations of the Franck–Condon factors for ionization which give the expected vibrational populations in HD^+. The following results (for rotational quantum number $N=0$) were obtained by Tadjeddine and Parlant [7]:

$v=0$	$f=0{\cdot}06320$	$v=7$	$f=0{\cdot}05416$	$v=14$	$f=0{\cdot}00501$
1	0·12862	8	0·03859	15	0·00362
2	0·15732	9	0·02730	16	0·00261
3	0·15186	10	0·01928	17	0·00187
4	0·12845	11	0·01366	18	0·00129
5	0·10040	12	0·00972	19	0·00083
6	0·07480	13	0·00696	20	0·00045
				21	0·00013

The ground electronic state of HD^+ has a calculated dissociation energy D_0 of 21 516·073 cm^{-1} [8], but the first excited state is repulsive. These states correlate at infinite nuclear separation with the nearly degenerate dissociation limits, $H^+ + D$ and $H + D^+$ respectively. Consequently electronic excitation leads to photodissociation and a number of authors have studied the photodissociation produced by argon ion lasers operating in the visible region of the spectrum [9]. In these cases excitation from $v''=7$ to 12 to the repulsive state occurs but it is clear that since the vibrational levels close to the dissociation limit are populated, even an infrared laser can produce photodissociation. This point was realized independently by Fournier *et al.* [10] and photodissociation produced by a carbon dioxide laser operating at 950 cm^{-1} was observed in our laboratory 3 years ago. Subsequent calculations [10] of the photodissociation in the infrared region spanned by a CO_2 laser show that $v=18$ is expected to have the largest cross-section, whilst for $v=19$, 20 and 21 the cross-sections are much smaller but rise with decreasing laser energy. As we shall show, our results are in at least qualitative agreement with these predictions.

Observation of the infrared photodissociation is readily achieved using a tandem mass spectrometer in which the photofragment H^+ or D^+ ions are separated from the parent HD^+ ions using either a magnetic analyser as described in our earlier paper [5] or an electrostatic analyser as used in the present work. When the infrared laser beam is collinear with the ion beam the D^+ and H^+ photofragment peaks do not exhibit structure. If, however, the laser beam is perpendicular to the ion beam with the electric vector in the ion beam direction, the photofragment peaks are readily resolved into doublets (see § 4). The structure arises from forward and backward scattered fragment ions, and proves that the photodissociating transition is polarized along the internuclear axis, as expected. The photofragment peak intensity is much higher for collinear interaction, however, so that we prefer to use this orientation for most of the work described in this paper.

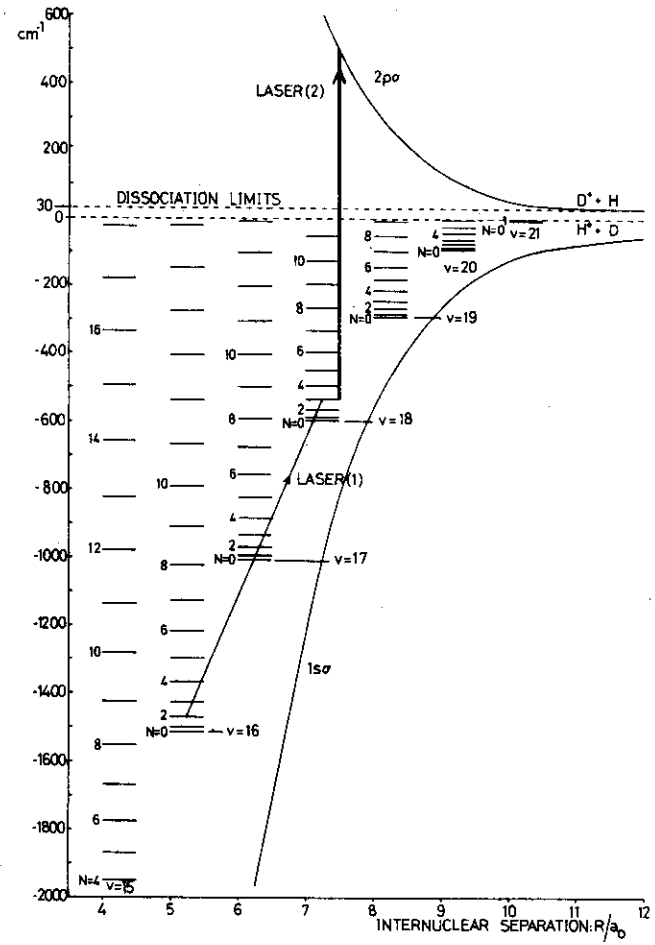

Figure 1. Principles of the two-photon infrared dissociation technique for HD^+.

Measurement of the photocross-section is of interest but it does not yield spectroscopic information directly. It does, however, suggest a route by which infrared absorption spectra can be obtained. Figure 1 illustrates the principles of our method. HD^+ ions in, for example, $v = 16$ lie too far below the repulsive electronic state to be dissociated by single photons in the CO_2 laser region (880 to 1080 cm^{-1}). However if resonant vibration–rotation transitions from $v = 16$ to 18 can be pumped with a laser, this excitation will be detected by an increase in the photofragment H^+ or D^+ peaks, since an ion in $v = 18$ is readily dissociated by absorption of a further photon. As we reported in our preliminary paper, this technique is successful and several rotational components of the $v = 18$–16 band system were detected with good signal-to-noise ratios. With the new apparatus described in this paper we have been able to observe further transitions, improve the accuracy of our measurements, and also improve the resolution.

Two advantages of using ion beams in which the molecules are moving rapidly will be mentioned here and discussed in more detail later. First, for collinear interaction of the ion and laser beams there is a large Doppler shift; spectroscopic scanning can be achieved very easily by using a fixed-frequency laser but sweeping the ion beam potential (and hence velocity). Second, an effect known as kinematic compression becomes more important the higher the ion beam potential, and results in very large reductions of the Doppler width which would otherwise be observed. The technique therefore yields spectra of high resolution, ultimately a desirable aspect, but one which makes the initial search problem much more difficult.

3. Experimental methods

The ion beam apparatus used in this work is a Vacuum Generators ZAB 1F instrument with modifications which make it more suitable for our work. The details of the apparatus are shown schematically in figure 2. A mixture of hydrogen and deuterium in equal proportions flows over a heated palladium catalyst and into an electron bombardment ion source which is gas tight apart from the ion exit slit and holes for the electron beam. We normally operate at a gas pressure inside the source of 1 mtorr and an electron beam energy of 60 to 100 eV. The source potential may be varied from 0 to + 10 kV and the ion beam is accelerated by collector and collimating slits which are at earth potential. The ion beam is analysed by a 55° electromagnetic sector of 30 cm radius which produces a focus at the intermediate slit. Immediately after the slit the ions can be detected by means of an off-axis electron multiplier. Consequently the mass spectrum of the source gas is recorded in the single focus mode and displayed on an oscilloscope by means of a scanning voltage applied either to the source or to the magnet. We adjust the gas pressures, ion source conditions and focusing and deflection lenses to optimize the HD^+ beam current; the source potential and magnet current are then fixed to permit transmission of the HD^+ beam, with rejection of other ions formed in the source or prior to the magnetic sector.

After the intermediate slit the ion beam passes through an 81·5° electrostatic analyser of 30 cm radius and is detected by either a second off-axis electron multiplier or a Faraday cup situated on the beam axis. The electrostatic analyser (ESA) voltage may be swept rapidly to permit oscilloscope display of

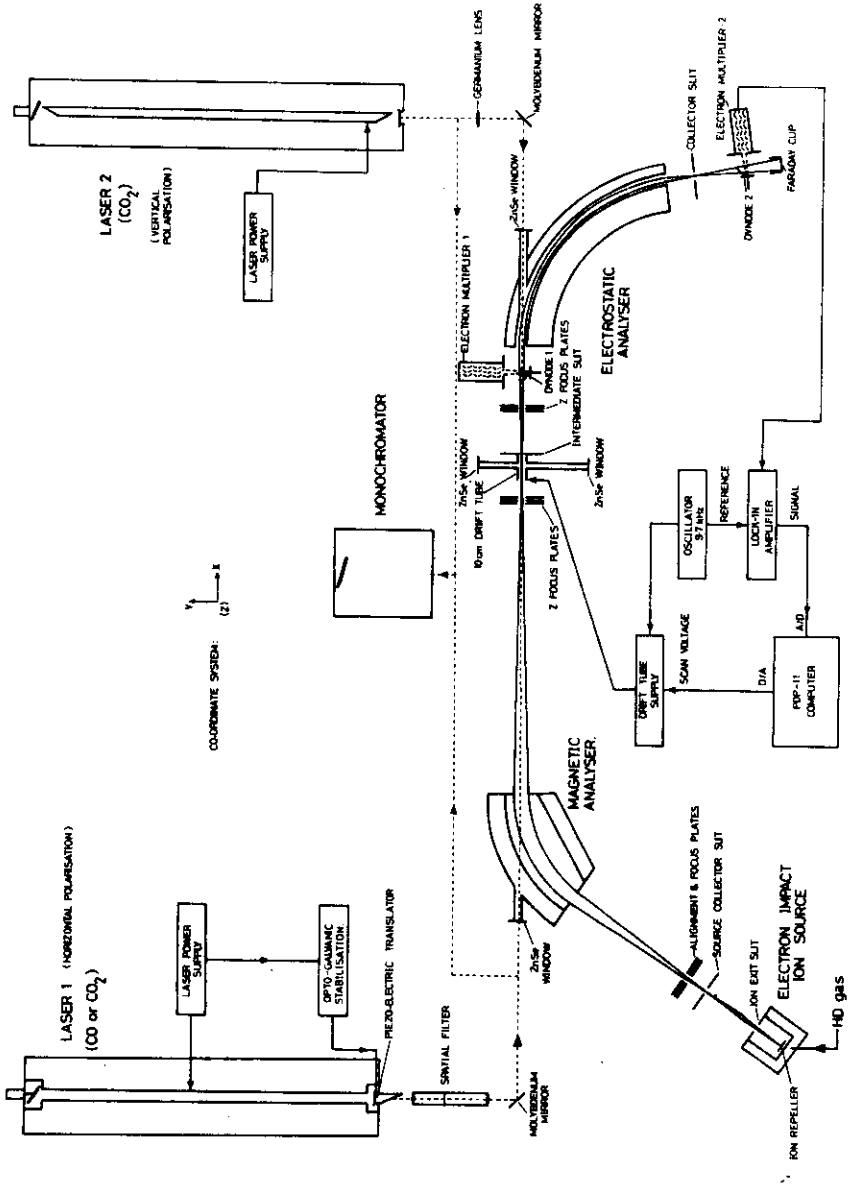

Figure 2. Block diagram of the apparatus.

the HD^+ ion beam peak shape and intensity. Optimization of the ion source conditions and subsequent ion optics yields a maximum HD^+ ion beam current of 10^{-7} A (6×10^{11} ions s^{-1} beam flux) at the Faraday cup.

Immediately before the intermediate slit the ion beam passes through a cylindrical tube of 10 cm length, which we shall refer to as the drift tube. Fragment ions formed between the magnetic and electrostatic sectors can be separated from the parent ions by appropriate adjustment of the ESA voltage and detected by means of a second off-axis electron multiplier. Application of a positive or negative potential to the drift tube results in splitting of the H^+ and D^+ peaks detected after the electrostatic analyser so that fragment ions formed in the drift tube are readily separated from those formed elsewhere at earth potential. The ESA voltage may therefore be set so that only fragment ions formed in the drift tube are detected; moreover if the potential applied to the drift tube is scanned, the ESA voltage may be swept synchronously to permit continuous detection of the drift tube fragment ions.

The ion beam apparatus is provided with four windows to allow interaction of the ion beam with one or more laser beams. Two of these windows are situated on the axis of the ion beam in the drift tube so that the ion and laser beams can interact collinearly, either parallel or antiparallel. The flight tube through the magnetic sector is modified to allow passage of the laser beam, and one of the ESA plates has a viewing aperture for the same purpose. So far as we can ascertain the performance of the ESA is not seriously degraded by this aperture but our application does not normally require high energy resolution. Two more windows are provided to allow perpendicular interaction of the laser beam with the ion beam, just before the intermediate slit in the drift tube region. All four windows are made of zinc selenide and have an anti-reflection coating optimized for radiation of 10 μm wavelength.

The collector slit before the magnetic sector, the intermediate slit and the collector slit after the ESA may all be varied in width from 0·05 to 2·5 mm; for high mass or energy resolution one would work with reduced slit widths but in the present work we have found it easier to work under conditions of low resolution with the slits fully open. The ion beam is focused by the magnetic sector to a width of 0·3 mm in the y direction at the intermediate slit. In addition the machine is equipped with z focus lenses situated 25 cm on either side of the intermediate slit, which can be adjusted to produce a crossover point so that the z dimension at the focus is 1 mm. However we have observed that full use of these lenses has an effect comparable to that of reducing the intermediate slit width. The effective resolution of the ESA is increased, which might be desirable in some applications but creates other problems in our experiments. Consequently we usually choose to work with little z focusing.

The high vacuum system is pumped by three oil diffusion pumps with appropriate rotary backing pumps. A 160 mm diffusion pump is situated directly below the ion source and a 100 mm pump is attached to the separating chamber between the ion source and magnetic sector. An additional 100 mm pump is attached to the chamber containing the drift tube. Under normal operating conditions with an ion beam of full intensity the background pressure in the drift tube region is 7×10^{-8} torr. Consequently fragment ions arising from collision-induced dissociation are negligible compared with those due to photodissociation.

We use two infrared lasers which are situated on either side of the ion beam apparatus as shown in figure 2. Laser (1) is an Edinburgh Instruments PL3 laser which can be used with either carbon monoxide or carbon dioxide as the lasing gas; for the measurements described in this paper it was used only as a CO_2 laser. The laser tube is sealed and laser line selection is achieved by rotation of a grating. Maximum output powers on the strongest lines are typically 25 W cw but the output power can be easily reduced to 1 or 2 W by adjustment of the gas pressure or discharge current. A gas mixing manifold attached to the laser head enables ready changes between $^{12}CO_2$ and $^{13}CO_2$ as the lasing gas and most of the measurements described in § 5 were made using $^{13}CO_2$. The laser frequency is locked to the peak of the gain curve by optogalvanic stabilization and the short term instabilities are estimated to be 100 kHz. Laser (2) is an Edinburgh Instruments PL4 CO_2 laser which can be operated either sealed off or with flowing gas; in the latter mode output powers on the strongest laser lines are over 40 W cw. This laser also uses a rotatable grating for line selection and optogalvanic stabilization. Laser line identification for both lasers is achieved by means of an Optical Engineering Ltd. Spectrum Analyser, which is actually a grating monochromator.

In most of our measurements laser (2) is operated at maximum power to optimize the photodissociation of the HD^+ ion beam. Laser (1) is used as the spectroscopic probe laser and is tuned to the wavelength required for inducing spectroscopic transitions. Spectroscopic scanning is achieved by sweeping the ion beam potential and at 10 μm wavelength a change in the ion beam potential from 1 to 10 kV corresponds to a Doppler tuning range of about 2 cm^{-1}. Since the spacings between adjacent CO_2 laser lines are 1 to 3 cm^{-1} we obtain almost continuous frequency coverage from 880 to 1080 cm^{-1} for parallel alignment alone; where gaps occur they can be accommodated by using antiparallel alignment of the laser and ion beams. In this case the roles of the two lasers can be reversed. When crossed-beam irradiation is required this can be achieved using either laser beam.

The beam from laser (1) is horizontally polarized and passes through a spatial filter consisting of two identical lenses (focal length 15 cm) separated by a pinhole whose position is adjustable. The position of the second lens is adjusted to produce a focus at the intermediate slit in the ion beam machine, which is located 2 m from the lens. Before entering the ion beam apparatus through one of the windows the beam is reflected through 90° by means of a molybdenum mirror; the laser beam is aligned to be parallel to the ion beam to within a tenth of a degree.

The beam from laser (2) is usually vertically polarized and is also reflected through 90° by means of a molybdenum mirror before entering the ion beam machine. It passes through a zinc selenide lens of focal length 100 cm situated to produce a focus at the intermediate slit. We have experienced some amplitude instability problems arising from interaction between the two lasers but these are greatly reduced by using crossed polarization as described previously. In addition we deliberately align laser (2) so that although the beam passes cleanly through the ion beam machine, it crosses the path of the beam from laser (1) at a sufficient angle, about 0·5°, to avoid interference with laser (1), and vice versa.

Photodissociation of the HD^+ beam is observed by adjusting the ESA potential so that photofragment H^+ or D^+ ions are selected and detected by the second off-axis electron multiplier. For the spectroscopic studies described in this paper we monitor the D^+ photofragment beam and, as described earlier, application of an appropriate potential (usually +100 to +300 V) to the drift tube identifies the D^+ ions formed in the drift tube. Oscilloscope display of the D^+ beam intensity facilitates the alignment of both laser beams to maximize the photofragment yield. If we do not use the z focus lenses the drift tube D^+ peak is smaller than the earth D^+ peak by a factor of 3. Use of the z focusing facility reverses this situation but creates instability problems. The sum of the photofragment H^+ and D^+ peak intensities indicates that about 0·01 per cent of the parent HD^+ beam is photodissociated by 30 W of cw laser power at 950 cm^{-1}.

We search for vibration–rotation transitions by setting laser (1) to a chosen laser line, maximizing the power of laser (2) and scanning the ion beam potential. The ion source potential is fixed, the magnet current is set to transmit the HD^+ beam and a slowly scanning voltage is applied to the drift tube. Superimposed upon the scan voltage is a square-wave modulation of frequency 9·7 kHz and amplitude ranging from 1 to 10 V. The D^+ ion beam current detected by the second multiplier is fed to a Brookdeal 9501 phase-sensitive detector which is referenced at the modulation frequency. The ESA voltage is synchronously scanned and modulated so that we always monitor the D^+ peak intensity. Typically we scan the drift tube from +300 to +500 V maximum; we start each scan with a +300 V offset (rather than 0 V) so that the drift tube and earth photofragment peaks are always well separated. After each drift tube scan the source potential and magnet current are reset, and the process repeated.

Modulation of the drift tube voltage corresponds to velocity modulation of the ion beam and is a satisfactory but not ideal way of discriminating in favour of the velocity-dependent resonant transitions. It is more satisfactory than mechanical chopping of the laser beam, which would modulate the photofragment background as well as the signal. A better alternative, at least in principle, would be to modulate the laser frequency. We are, however, not able to obtain sufficient modulation amplitude at frequencies above a few Hz, and we are also then unable to use optogalvanic stabilization. If our sensitivity were limited by the ion beam statistical noise it would, of course, be unnecessary to use any modulation scheme. Unfortunately our noise is about three times larger than the shot noise limit, even at a detection frequency of several kHz.

The scanning and data processing operations are controlled by a DEC MINC11 minicomputer system. All of the voltage supplies for the ion beam machine are programmable but at present we use the computer to control only the drift tube voltage and to read the d.c. output of the phase-sensitive detector. We have also used the computer to generate the square-wave modulation, read the electron multiplier output directly and perform in software most of the functions of a lock-in amplifier. In practice we find a small advantage in signal-to-noise ratio is obtained by using an external oscillator and phase-sensitive detector. The program for initiating the scanning conditions and processing the output data is written in FORTRAN, whilst those sections which control real-time operations are written in assembly language, MACRO-11. When searching for new resonance lines we usually scan the drift tube voltage in 1 V s^{-1} steps; for high resolution and sensitivity, however, we have used 25 s integration times combined with 0·1 V or smaller increments.

The ion source potential is measured continuously by means of a digital voltmeter and the drift tube potential is programmed directly by the computer. Both of these potentials are known to an accuracy better than 1 V although, as we shall show later, the final ion beam potential is not quite equal to the sum (or difference) of the source and drift tube potentials. Nevertheless we are able to determine the absolute value of the ion beam potential (which determines the Doppler shift and resulting transition frequency) to better than 1 V accuracy, leading to high precision in the determination of the spectroscopic transition frequencies.

Finally in this section we draw attention to the main differences between the experimental techniques described above and those used in our initial observation of the HD^+ spectrum reported previously [5]. The earlier ion beam machine was much smaller and employed two 90° magnetic sectors of 6 cm radius. We were not able to perform synchronous scanning of the drift tube and analyser magnet and, most importantly, we had only one infrared laser available. The new machine is more versatile, is stable over periods of many hours, and is fully compatible with computer monitoring and control.

4. Experimental results

We have carried out preliminary studies of the photofragmentation produced by crossed-beam irradiation, combined with kinetic energy analysis of the photofragment H^+ ions. We can obtain kinetic energy spectra either by sweeping the ESA voltage, or by keeping the ESA voltage fixed and scanning the drift tube potential. In practice we find the latter procedure to be more convenient because the drift tube scans can be performed with the full 12-bit resolution of our D/A converter. Figure 3 shows a proton kinetic energy spectrum obtained with the collector slit reduced in width so as to reduce the acceptance angle of the fragments. Spectra of much higher signal-to-noise ratio can be obtained

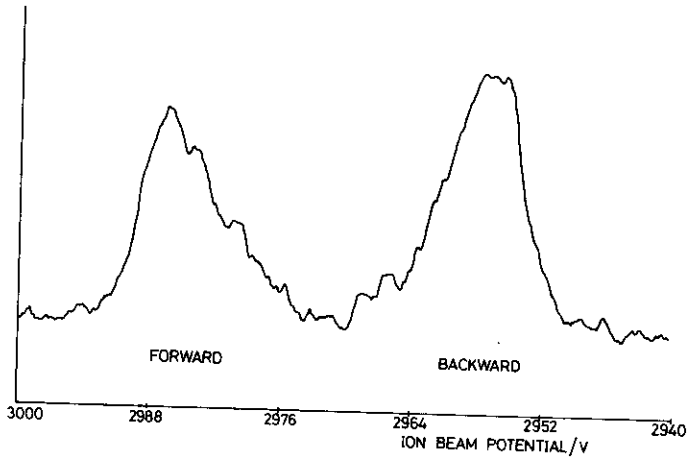

Figure 3. Kinetic energy spectrum of photofragment protons from the photodissociation of HD^+ at 944·1940 cm^{-1}

with a wider collector slit, at the price of poorer resolution. The most prominent feature is the separation of the peaks due to forward and backward scattered protons, confirming that the polarization of the electronic dissociating transition is along the HD^+ internuclear axis as expected. We also observe evidence of structure arising from excitation from different vibration–rotation levels of the ground state. We hope to improve the resolution and will report the results elsewhere; it may be possible to determine relative values of the photocross-sections for different vibration–rotation levels, and to compare the relative yields of protons and deuterons. It is of interest to note that because the centre-of-mass energy of the fragments is small (0·12 eV or less), the energy resolution obtainable is much higher than in the case of dissociation with an argon ion laser operating in the visible region.

Our initial searches for rotational components of the $v=18$–16 band were based upon the predictions of Hunter *et al.* [11]. The more recent and more accurate data of Wolniewicz and Poll [8] has simplified the search problem and we have now observed the first seven members of the R-branch and the first two members of the P-branch. In most cases laser (1) is used as the spectroscopic probe laser, and the ability to use both $^{12}CO_2$ and $^{13}CO_2$ has provided increased spectral coverage. Most of our measurements have been made with 10 W cw power from the resonant laser (1) and 30 W cw power from laser (2) to maximize the D^+ photofragment beam intensity. For three of the components ($R(0)$, $R(2)$ and $R(3)$) we were able to drive the same vibration–rotation transition using three different laser lines in either parallel or antiparallel collinear orientation. In four other cases we were able to use two different laser lines and only for $R(6)$ and $P(2)$ are we confined to a single measurement. We have also observed one component ($R(7)$) of the $v=17$–15 band; here, too, we have only one measurement.

Table 1 gives the details of our measurements with the laser lines used in each case; the laser frequencies are taken from the recent work of Freed *et al.* [12]. We always sweep the drift tube with an increasing positive potential so that the resonant value of the ion beam potential is obtained by subtracting the resonant drift tube potential from the ion source potential. The values of the ion beam potential are then used to calculate spectroscopic transition frequencies by means of the relativistic Doppler shift formula

$$\nu_{res} = \nu_{laser} \left\{ \frac{1 \mp v/c}{1 \pm v/c} \right\}^{1/2},$$

where the upper signs apply to parallel orientation of the laser and ion beams, and the lower signs are for antiparallel alignment. v is the ion velocity at the resonant beam potential and is calculated using the values of the fundamental constants listed by Cohen and Taylor [13].

After the measurements were completed we found that for the same vibration–rotation transition the antiparallel alignment always gave a higher value for the transition frequency than the parallel alignment. The results were reproducible and systematic in that the discrepancies were larger for higher beam potentials. This effect would arise if the laser and ion beams were not exactly collinear; however this explanation was easily rejected because the angle between the beams would need to be 4° to account for the discrepancies, and the dimensions of the ion beam machine are such that once the laser beam is

Table 1. Experimental and theoretical vibration–rotation frequencies in the HD^+ ion.

Lower v'', N''	Upper v', N'	Laser line Isot.	Laser line N	Laser freq./ cm^{-1}	Alignment	Ion energy/ eV	Exp. freq./ cm^{-1}	Final exp. freq./ cm^{-1}	Theor. freq./ cm^{-1}	(Exp–theory)/ cm^{-1}
16, 0	18, 1	12	P(36)	929·0174	*P*	10444·7	926·4896	926·4895	926·490	0·000
		12	P(40)	924·9740	*A*	3772·2	926·4898			
		13	R(20)	928·6567	*P*	7682·7	926·4892			
16, 1	18, 2	13	R(28)	933·8807	*P*	4437·0	932·2237	932·2237	932·220	+0·004
		12	P(34)	931·0014	*A*	2421·6	932·2236			
16, 2	18, 3	13	R(30)	935·1358	*P*	5961·8	933·2128	933·2129	933·207	+0·006
		12	P(30)	934·8945	*P*	4558·5	933·2132			
		12	P(34)	931·0014	*A*	7917·6	933·2126			
16, 3	18, 4	12	P(38)	927·0083	*A*	8184·4	929·2468	929·2471	929·238	+0·009
		12	P(34)	931·0014	*P*	5002·4	929·2476			
		13	R(24)	931·3092	*P*	6914·3	929·2469			
16, 4	18, 5	12	R(6)	918·7440	*A*	3063·5	920·1007	920·1001	920·089	+0·011
		13	R(10)	921·6753	*P*	4119·5	920·0995			
16, 5	18, 6	13	P(8)	907·0528	*P*	4030·0	905·5190	905·5191	905·512*	+0·007*
		13	P(12)	903·7497	*A*	5383·6	905·5192			
16, 6	18, 7	13	P(32)	886·0614	*P*	1275·0	885·2183	885·2183	885·229*	−0·011*
16, 1	18, 0	13	P(12)	903·7497	*P*	8242·1	901·5649	901·5648	901·571	−0·006
		13	P(16)	900·3686	*A*	2479·3	901·5646			
16, 2	18, 1	13	P(34)	884·1843	*P*	3806·0	882·7312	882·7312	882·743	−0·012
15, 7	17, 8	12	R(24)	1081·0874	*P*	6021·6	1078·8532	1078·8532	1078·907*	−0·054*

P denotes parallel alignment of the laser and ion beams, *A* denotes antiparallel. Theoretical frequencies marked with an asterisk were not listed by Wolniewicz and Poll [8], but have been calculated by us from the *B*, *D* and *H* constants which can be derived from Wolniewicz and Poll's data.

focused cleanly through the apparatus, the ion and laser beams are necessarily parallel to within 0·1°. We are now certain that the discrepancies arise because the true ion beam potential in the field-free regions is not exactly equal to the measured ion source potential. The source is floated at a positive potential and the ions accelerated out by the potential gradient created by the extraction and collimating slits which are at earth potential. Clearly there is some field penetration into the source, so that the ions are not formed in a region of zero potential with respect to the ion source block. If this explanation is correct we must apply a multiplying correction factor to determine the true ion beam potential; a single value of the correction factor must hold for all values of the source potential and should bring the parallel and antiparallel measurements into agreement. We find this to be the case, the correction factor being 0·9953, and the corrected values of the ion beam energy are listed in table 1. The resonant frequencies calculated from these corrected values are also listed in table 1 and the internal consistency of our results is excellent. The final average values of the transition frequencies are given in table 1, the experimental uncertainty being $\pm 0{\cdot}0005\ cm^{-1}$.

Independent verification of the correction factor is obtained by recording the ESA voltage required to focus H_2^+, HD^+ and D_2^+ ions, and its dependence on the ion source potential. The dimensions of the ESA (the radius and plate separation) are known with sufficient accuracy that the measured ESA voltage may be used to calculate the true ion beam potential, which may then be compared with the measured value. These measurements confirm a correction factor of 0·995.

Figure 4 (*a*) shows the 18, 3–16, 2 line obtained with a laser (1) power of 14 W, the spectrum is calibrated in MHz and the observed linewidth is 35 MHz. As the power of laser (1) is reduced (with the power of laser (2) maintained at 30 W) the line width decreases and the line is observed to split into two components as shown in figure 4 (*b*). All nine components of the $v = 18$–16 band show similar behaviour with the splitting between the components ranging from 14 to 20 MHz. The splitting is due predominantly to the difference in proton Fermi contact interaction for the lower and upper vibrational levels, as we shall show in the next section. With a laser (1) power of 1·4 W the width of the weaker component is 7·3 MHz, whilst the stronger component is somewhat broader at 10·4 MHz. These results demonstrate the high resolution which is obtainable because of the kinematic compression effect mentioned in § 2. A dispersion in the parent ion beam energy of $\pm 0{\cdot}5$ V would yield a Doppler width of 4·8 MHz at a beam potential of 6000 V, but at a beam potential of 10 V, the corresponding linewidth would be 2534 MHz (for a transition frequency of 1000 cm^{-1}). In fact the residual linewidths we observe could still be dominated by laser power broadening, or arise from unresolved structure due to spin–rotation interaction (plus deuteron hyperfine interaction for the stronger component) which we shall discuss further in the next section. We need to improve our signal-to-noise ratio in order to reduce the laser power further.

The best signal-to-noise ratio is observed for the 18, 3–16, 2 line and the signals become weaker as the rotational quantum number increases. Since we do not at present have experimental or theoretical information about the rotational dependence of the photocross-sections, we cannot make a precise determination of the rotational population factors in the HD^+ beam. Our results do

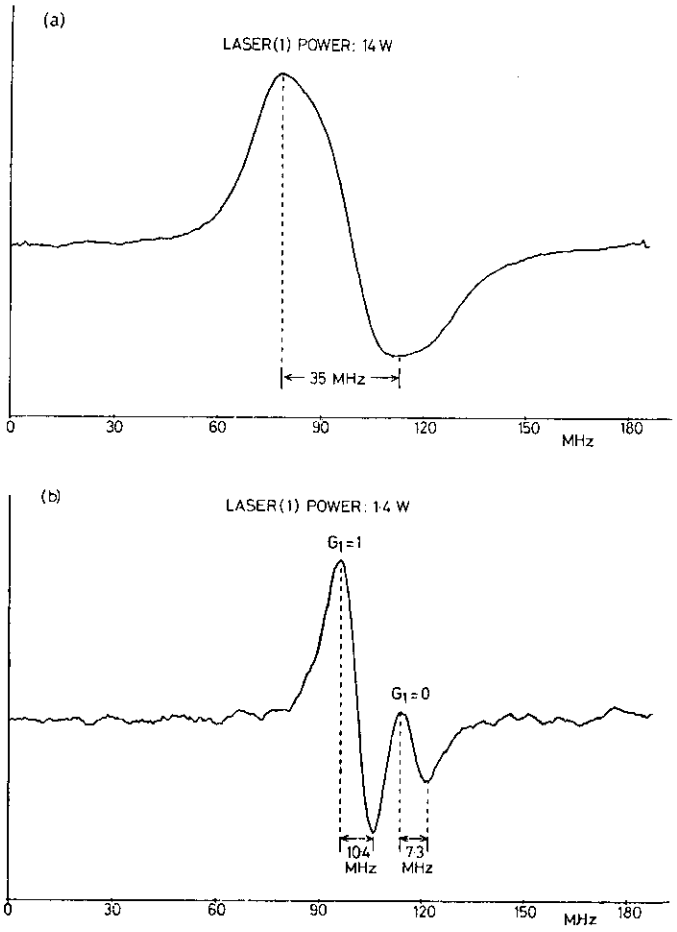

Figure 4. Observations of the 18, 3–16, 2 transition of HD^+ using the $P(30)$ laser line of $^{12}CO_2$ at 934·8945 cm^{-1}. (*a*) High laser power. (*b*) Low laser power, showing proton hyperfine splitting.

suggest, however, that the rotational populations are not too different from those calculated by assuming thermal distribution for neutral HD at the source temperature. In other words, the electron impact ionization process causes very little rotational excitation.

5. Theoretical analysis

Although a large number of calculations have been performed for the hydrogen molecular ion, only two papers give predictions for the highest vibration–rotation levels of HD^+ which are probed by our experiments. Hunter, Yau and Pritchard [11] list values of the energies of all the vibration–rotation levels of the ground state, but comment on the particular difficulties which arise in

HD^+, as compared with H_2^+ and D_2^+, associated with the existence of two dissociation limits which differ in energy by 29·8 cm^{-1} (that is, $H^+ + D$ and $H + D^+$). Hunter *et al.* anticipated errors of up to 15 cm^{-1} in their calculations of the levels close to the dissociation limit. Our measurements, which give energy differences between vibration–rotation levels actually agree with Hunter, Yau and Pritchard's calculations to within 0·2 cm^{-1} on average.

The other paper which is of direct relevance to our work is that of Wolniewicz and Poll [8] who have calculated the energies of the bound vibration–rotation levels up to $N=5$. Their predictions for the lower levels ($v=0$ to 3) have already been compared with the measurements of Wing *et al.* [4], and theory and experiment agree to within a maximum discrepancy of 0·003 cm^{-1}. However, measurements on the levels close to the dissociation limit provide a particularly severe test of the theory, because some of the non-adiabatic effects become increasingly important.

Wolniewicz and Poll list theoretical energies for $N=0$ to 5 for $v=0$ to 20, and $N=0$ and 1 for $v=21$. There are at least two different methods of comparing our experimental results with the theory. The simplest is to calculate the appropriate energy differences from Wolniewicz and Poll's data and to compare predicted and measured transition frequencies. This comparison is presented in the final column of table 1. We see that for the R-branch up to $R(4)$ the experimental frequencies are progressively higher (to a maximum difference for $R(4)$ of 0·011 cm^{-1}), whilst the P-branch experimental frequencies are progressively lower. Unfortunately we are only able to observe $P(1)$ and $P(2)$, the further members of the branch being at frequencies lower than our laser can provide. Clearly the discrepancy between experiment and theory is systematic, and we turn to the second method of comparison, which is in terms of the molecular parameters involved. We have analysed our data for the $v=18$–16 band in terms of the standard expression [14]

$$\nu = \nu_0 + (B_{16}+B_{18})m + (B_{18}-B_{16}-D_{18}+D_{16})m^2 - (2D_{18}+2D_{16}-H_{18}-H_{16})m^3 - (D_{18}-D_{16}-3H_{18}+3H_{16})m^4 + (3H_{18}+3H_{16})m^5 + (H_{18}-H_{16})m^6,$$

where $m=N+1$ for the R-branch and $m=-N$ for the P-branch. B_v, D_v and H_v are the usual rotational and centrifugal distortion constants and ν_0 is the vibrational energy separation between $v=16$ and 18. We have carried out a least-squares analysis of our nine measurements using the seven constants in the above equation, and the resulting values are given in table 2. The error limits

Table 2. Molecular constants for $v=16$ and 18. Experimental values are from a least-squares analysis of our data. Theoretical values are from a least-squares analysis of the rotational energies calculated by Wolniewicz and Poll [8].

	$\{G(18)-G(16)\}$/ cm^{-1}	B_{16}/ cm^{-1}	$D_{16}\times10^3$/ cm^{-1}	$H_{16}\times10^6$/ cm^{-1}	B_{18}/ cm^{-1}	$D_{18}\times10^3$/ cm^{-1}	$H_{18}\times10^6$/ cm^{-1}
Experiment	916·2081 ±0·0003	7·33605 ±0·00020	7·211 ±0·025	7·8 ± 1·4	5·15624 ±0·00020	7·759 ±0·025	3·2 ± 1·4
Theory	916·212	7·33476 ±0·00010	7·280 ±0·011	3·1 ± 0·3	5·15460 ±0·00008	7·738 ±0·008	0·4 ± 0·2

are calculated on the basis of one standard deviation, and the values given for the constants reproduce our experimental frequencies to within a maximum deviation of $\pm 0{\cdot}001$ cm^{-1}. We realize that further observations for higher N would be desirable, but they are beyond the range of our laser. We have carried out a similar least-squares analysis of the theoretical data of Wolniewicz and Poll. The five rotational energies for each vibrational level are used to calculate B, D and H constants and the results are also given in table 2. We have used the theoretical values of the molecular constants to provide predictions for $R(5)$ and $R(6)$, which are marked with asterisks in table 1. Similar analyses of the theoretical data for $v=17$ and 15 can be used to predict the frequency of the 17, 8–15, 7 transition, as shown in table 1. Because the experimental data [4] for the $v=0$ to 3 levels does not extend beyond $N=2$, it is not possible to conclude that the theory is less accurate for levels of high v than for low v. It is clear that further experimental measurements involving levels of both lower and higher v (with N values as high as possible) are most desirable, and we shall indicate in the final section how they might be obtained.

We now turn to the nuclear hyperfine and spin–rotation interactions. Since our present data is limited we outline the main features only briefly. The nuclear hyperfine and spin–rotation hamiltonian may be written

$$\mathscr{H} = b_1\mathbf{I}_1 \cdot \mathbf{S} + b_2\mathbf{I}_2 \cdot \mathbf{S} + c_1 I_{1z} S_z + c_2 I_{2z} S_z + \gamma \mathbf{S} \cdot \mathbf{N}.$$

The first two terms represent the Fermi contact interaction between the electron spin ($\mathbf{S}$) and the proton ($\mathbf{I}_1$) and deuteron ($\mathbf{I}_2$) nuclear spins. The third and fourth terms represent the axial components of the dipolar hyperfine couplings, where z is the internuclear axis, whilst the fifth term represents the spin–rotation interaction. The simplified form of the dipolar terms implies neglect of non-axial components which have matrix elements connecting different electronic states.

The hyperfine and fine structure of each vibration–rotation level will therefore depend upon the values of the five constants b_1, b_2, c_1, c_2 and γ. Information about these constants in H_2^+ has been obtained for the levels $v=4$ to 8 by Jefferts [3], and Ray and Certain [15] have given theoretical calculations up to $v=8$. Extrapolation of their results to $v=16$ and 18 (a long extrapolation, admittedly) suggests that the Fermi contact interaction constant (b_1) for the proton is by far the most important, with a value of approximately 720 MHz. The deuteron constant b_2 would then be expected to be smaller in proportion to the difference in magnetogyric ratios for the proton and deuteron (i.e. by a factor of 0·1535). The dipolar constants c_1 and c_2 are fairly small for the lower vibrational levels and are likely to be even smaller for $v=16$ and 18. Finally the spin–rotation constant γ is only 32 MHz for $v=0$ and becomes progressively smaller the higher the vibrational level. We anticipate γ values for $v=16$ and higher of only a few MHz. These considerations suggest that the most appropriate coupling scheme for the spin and rotational angular momenta is the following:

$$\mathbf{S}+\mathbf{I}_1=\mathbf{G}_1, \quad G_1 = 1;\ 0,$$

$$\mathbf{G}_1+\mathbf{I}_2=\mathbf{G}_2, \quad G_2 = 2, 1, 0;\ 1,$$

$$\mathbf{G}_2+\mathbf{N}=\mathbf{F}, \quad F = |N+G_2|, \ldots, |N-G_2|.$$

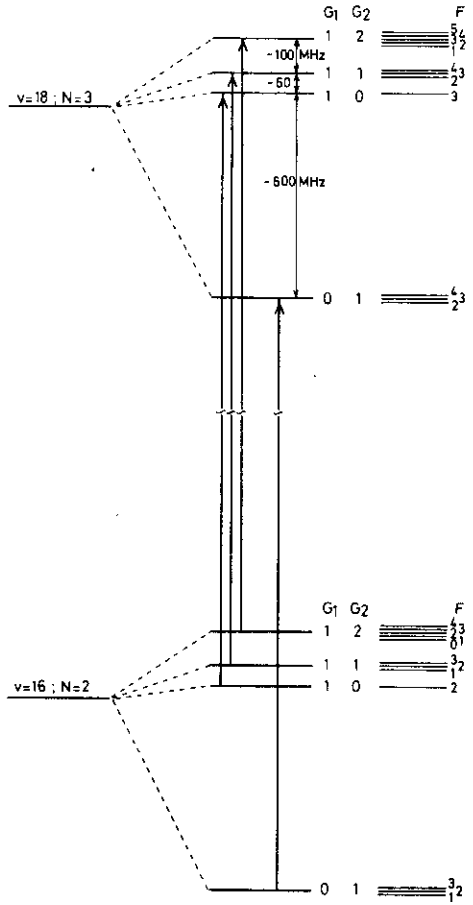

Figure 5. Energy level diagram for the 18, 3–16, 2 transition showing the expected nuclear hyperfine and spin–rotation structure.

Consequently the hyperfine levels may be characterized by values of the quantum numbers G_1, G_2, N, F and an appropriate energy level diagram for the transition 18, 3–16, 2 is shown in figure 5. One of the ultimate aims of our experiments is, of course, to determine the splittings between the levels and hence the values of the constants.

The selection rules for the electric-dipole allowed vibration–rotation transitions are $\Delta N = \pm 1$, $\Delta G_1 = \Delta G_2 = 0$, $\Delta F = \pm 1, 0$. The strongest lines therefore arise from the four transitions shown in figure 5, and any splitting between the lines will arise only from differences in the values of the constants for the two vibrational levels involved. The doublet splitting shown in figure 4 (b) therefore arises primarily from the difference in b_1 for $v=16$ and 18. The weaker component involves the levels with $G_1=0$, and the stronger component has $G_1=1$. The stronger component therefore contains unresolved deuteron

splitting (approximately seven times smaller than the observed proton splitting) which presumably accounts for its greater width. Each component is additionally broadened by unresolved spin-rotation splittings.

The values of the hyperfine constants would be determined by observation of the transitions for which $\Delta G_1 \neq 0$, $\Delta G_2 \neq 0$. Unfortunately these transitions have very little electric dipole intensity, essentially because the spin–rotation coupling is so weak. We shall discuss the chances of observing these transitions in the final section. The most interesting fact to emerge from our studies of the hyperfine splitting is that the separation between the components for the R-branch lines increases slightly with increasing N value. Since the components are inhomogeneously broadened by unresolved structure, however, it is important that we improve our resolution.

6. Discussion

In the previous section we compared our results with the predictions of the best available theory. It is clear that we must extend our measurements to higher v and N values, and thereby provide an even more severe test of the theory. Success will depend upon increasing the sensitivity of our experiments and fortunately there is scope for some improvement. Our present noise level is a factor of three higher than the shot noise limit, and we hope to increase the photofragment D^+ beam intensity through the use of a longer drift tube. The parent HD^+ beam intensity could also be considerably increased, since it is at present well below the space-charge limit. An overall increase in sensitivity would improve our chances of observing further transitions, and would also enable us to further probe the inherent resolution. At present the narrowest lines we have observed are 6 MHz wide, but we have not yet had sufficient sensitivity to reduce the laser (1) power to a level where power broadening is absent. It should be possible to reach the Doppler limit arising from dispersion in the ion beam energy. Higher spectroscopic resolution could then be obtained from experiments at lower frequencies (for example, using far infrared lasers).

At least three other vibrational bands of HD^+ are within the ranges provided by the CO_2 or CO laser. The $v = 19$–15 band is accessible with the CO laser whilst rotational components of the 20–17 and 21–17 bands can almost certainly be Doppler-tuned into resonance with CO_2 laser lines. The last bound level ($v = 21$, $N = 1$) is predicted by Wolniewicz and Poll to lie only 0·74 cm^{-1} below the lower dissociation limit, $H^+ + D$. Our aims are to determine whether $v = 21$, $N = 1$ is the highest bound level, to measure its energy, and to determine the hyperfine constants. We anticipate that a vibration–rotation level whose separation from the lower dissociation limit is small compared with the splitting between the dissociation limits (29·8 cm^{-1}) could exhibit novel hyperfine effects, in that the charge and electron spin distributions might no longer be symmetric with respect to the geometric centre of the nuclei.

All of our studies so far have used a low pressure electron impact ion source; the vibrational level populations in the HD^+ beam appear to be those predicted by Franck–Condon calculations, whilst the relative rotational level populations are those calculated for neutral HD at the source temperature. We shall shortly be installing a plasmatron ion source, which will almost certainly produce an HD^+ beam with a different population distribution; in particular much higher rotational levels are likely to be populated. There then arises the exciting possibility of studying the quasibound levels of HD^+ which lie above the dissociation limit but are metastable because of the centrifugal barrier to dissociation.

We are also planning experiments using pulsed laser operation because of the possibilities of detecting other types of transitions which would be driven by sufficiently high laser powers. These include the cross-hyperfine transitions ($\Delta G_1 \neq 0$, $\Delta G_2 \neq 0$) mentioned earlier, molecular quadrupole-induced transitions and especially multiphoton vibration–rotation transitions. Observation of multiphoton excitation in a simple molecule like HD^+ might shed some light on the complex excitation processes which are involved in the multiphoton dissociation or ionization of polyatomic molecules. The fact that all the vibrational levels of the HD^+ ion are populated by the initial electron impact ionization process provides total flexibility in the search for multiphoton transitions.

Finally we note that we have observed infrared photodissociation of a large number of other molecular ions, diatomic and polyatomic. The techniques described in this paper for studying vibrational levels close to the dissociation limit therefore appear to be of general applicability.

We wish to thank Professor W. H. Wing, Dr. J. M. Brown, Mr. R. H. Bateman and Mr. R. A. Kennedy for helpful discussions, and Mr. P. D. Francis for advice concerning computer programs. A.C. thanks the Royal Society for a Research Professorship and J. B. thanks the University of Southampton for a Research Fellowship. We are indebted to the Science Research Council for financial support, especially towards the cost of the equipment.

References

[1] Dehmelt, H. G., and Jefferts, K. B., 1962, *Phys. Rev.*, **125**, 1318.
[2] Richardson, C. B., Jefferts, K. B., and Dehmelt, H. G., 1968, *Phys. Rev.*, **165**, 80.
[3] Jefferts, K. B., 1968, *Phys. Rev. Lett.*, **20**, 39; 1969, *Ibid.*, **23**, 1476.
[4] Wing, W. H., Ruff, G. A., Lamb, W. E., Jr,. and Spezeski, J. J., 1976, *Phys. Rev. Lett.*, **36**, 1488.
[5] Carrington, A., Buttenshaw, J., and Roberts, P. G., 1979, *Molec. Phys.*, **38**, 1711.
[6] Carrington, A., 1979, *Proc. R. Soc.* A, **367**, 433.
[7] Tadjeddine, M., and Parlant, G., 1977, *Molec. Phys.*, **33**, 1797.
[8] Wolniewicz, L., and Poll, J. D., 1980, *J. chem. Phys.*, **73**, 6225.
[9] Van Asselt, N. P. F. B., Maas, J. G., and Los, J., 1975, *Chem. Phys.*, **11**, 253.
[10] Fournier, P., Lassier-Govers, B., and Comtet, G., 1979, *Laser-induced Processes in Molecules*, edited by K. L. Kompa (Springer-Verlag).
[11] Hunter, G., Yau, A. W., and Pritchard, H. O., 1974, *Atom. Data nucl. Data Tables*, **14**, 11.
[12] Freed, C., Bradley, L. C., and O'Donnell, R. G., 1980, *J. quant. Electron.*, QE **16**, 1195.
[13] Cohen, E. R., and Taylor, B. N., 1973, *J. Phys. Chem. Ref. Data.*, **2**, 663.
[14] Herzberg, G., 1950, *Spectra of Diatomic Molecules* (D. Van Nostrand Co. Inc.).
[15] Ray, R. D., and Certain, P. R., 1977, *Phys. Rev. Lett.*, **38**, 824.